Environmental Pollution 243 (2018) 1833–1845

Contents lists available at ScienceDirect

Environmental Pollution

journal homepage: www.elsevier.com/locate/envpol

Solid-phase distribution and mobility of thallium in mining-metallurgical residues: Environmental hazard implications☆

Javier Aguilar-Carrillo [a, *], Lidya Herrera [b], Emmanuel J. Gutiérrez [c], Iván A. Reyes-Domínguez [d]

[a] CONACyT - Department of Environmental Technology, Institute of Metallurgy, UASLP, 78210, San Luis Potosí, S.L.P, Mexico
[b] Department of Environmental Technology, Institute of Metallurgy, UASLP, 78210, San Luis Potosí, S.L.P, Mexico
[c] CONACyT - Department of Materials Engineering, Institute of Metallurgy, UASLP, 78210, San Luis Potosí, S.L.P, Mexico
[d] CONACyT - Department of Mineral Processing, Institute of Metallurgy, UASLP, 78210, San Luis Potosí, S.L.P, Mexico

ARTICLE INFO

Article history:
Received 2 July 2018
Received in revised form
20 September 2018
Accepted 2 October 2018
Available online 5 October 2018

Keywords:
Thallium partitioning
Labile fraction
Poorly-crystalline phases
Residues
Sediments
ICP-MS

ABSTRACT

Thallium (Tl) and its compounds are non-essential and highly toxic for living organisms, even at low concentrations. In this paper, we analyzed the presence and geochemical distribution of Tl in different mining-metallurgical and sediment samples collected from several mining zones of Mexico. A modified BCR sequential extraction procedure was also applied to the samples to investigate the geochemical behavior and potential environmental risk of Tl according to types of ore deposit and mineral processing method applied. Results revealed the presence of Tl in the majority of the mining-metallurgical samples, with labile concentrations reaching up to values of 184.4 mg kg^{-1}, well above the environmental standards. A comparison of Tl partitioning in different samples showed that Tl was usually found associated with labile fractions instead of entrapped in the environmentally-passive residual fraction. Specifically, high levels of Tl were extracted from the exchangeable/acid-extractable and poorly-crystalline reducible fractions, suggesting its association with both soluble and amorphous Fe-Mn oxyhydroxides, respectively. Besides, Tl was also frequently found associated with the crystalline reducible fraction, presumably bonded to manganese oxides and jarosite-like minerals. Lastly, little amounts of Tl were extracted from the oxidizable fraction. Considering the fractionation of Tl in these mining-metallurgical samples, they may pose a significant environmental hazard. This study provides useful insights into the potential sources of Tl pollution in Mexico and emphasizes the need for further research to determine the extent of its impact and to develop effective remediation protocols to protect the environment from Tl toxicity.

1. Introduction

Mining and metallurgical activities have been developed almost everywhere that humans have settled, generating significant volumes of residues and thus resulting in the emission of unexpectedly large amounts of metals and metalloids into the environment (Camizuli et al., 2018). Weathering of mining-metallurgical residues is a worldwide environmental concern, as they can act as a potential long-term source of pollutants, enabling the contamination of soils, sediments, and ground and surface waters, thereby affecting entire ecosystems.

In recent years, there has been an increasing research interest in the environmental geochemistry of thallium (Tl), a non-essential metal which shows greater acute and chronic toxicity than other elements such as As, Hg, Cd, or Pb in most living organisms (Nriagu, 1998). As a consequence, it has been included in the USEPA priority pollutant list (USEPA, 2014). Although Tl concentrations in terrestrial environments range from 0.1 to 2 mg kg^{-1}, with an average content of Tl in the continental crust of 0.49 mg kg^{-1} (Kabata-Pendias, 2011), it occurs at higher concentrations in metallogenetic epithermal environments (<200 °C) associated with sulfide minerals and igneous rocks due to its unique chalcophile and lithophile geochemical properties (Martin and Kaplan, 1998; Karbowska et al., 2014; Belzile and Chen, 2017). This dual character makes Tl to be naturally found in sulfides and silicates resembling the chemical behavior of other chalcophile (Pb, Zn, Cu, Hg, As, Sb)

☆ This paper has been recommended for acceptance by B. Nowack.
* Corresponding author.
E-mail addresses: javier.aguilar@uaslp.mx (J. Aguilar-Carrillo), lidyahg@alumnos.uaslp.edu.mx (L. Herrera), emmanuel.gutierrez@uaslp.mx (E.J. Gutiérrez), alejandro.reyes@uaslp.mx (I.A. Reyes-Domínguez).

https://doi.org/10.1016/j.envpol.2018.10.014
0269-7491/

and lithophile (K, Rb, Cs, Na) elements (Peter and Viraraghavan, 2005; Gomez-Gonzalez et al., 2015a; Liu et al., 2016). For instance, the well-known mechanism of Tl toxicity to biota is related to the non-discriminatory uptake of Tl^+ instead of K^+ due to their similar ionic radii (Peter and Viraraghavan, 2005; Grosslova et al., 2015). Despite Tl intoxication being rare (Jia et al., 2013), industrial activities focused on the mining and processing of Tl-hosting mineral deposits with valuable and highly sought-after metals, such as Au, Ag, Cu, Pb, Zn, Hg or U, are responsible for the release of large amounts of anthropogenic Tl into the environment (Lis et al., 2003; Casiot et al., 2011; Vaněk et al., 2013; Vaněk et al., 2015). As a case in point, Tl is present in most rivers draining metal mining areas in concentrations of 1–828 mg L^{-1} (Belzile and Chen, 2017). Particularly, activities like roasting Tl-rich polymetallic sulfides (i.e., pyrite or sphalerite for sulfuric acid production), coal combustion and cement production are significant sources of Tl pollution (Lopez-Arce et al., 2017, and references therein). In all these processes, Tl could either be volatilized or incorporated into crystalline phases, and subsequent weathering of these solids outcomes in Tl solubilization or migration associated with fine particles. According to the International Programme on Chemical Safety (IPCS, 1996), 2000–5000 tons of Tl were estimated to be discharged annually from industrial processes, although this estimation did not include the discharge of Tl in China, which owns most of the Tl-rich mineral resources in the world (Xiao et al., 2012). Thallium recycling and pollution controls have hardly been considered in related industrial activities, and Tl contamination has been studied only to a limited extent due to its very low content in the environment, which hinders its analysis (Liu et al., 2016). Fortunately, the development of monitoring methods and analytical techniques (i.e., ICP-MS) with Tl detection limits in the low ng L^{-1} or tenth of pM in solution, has become a widespread and useful tool concerning the industrial contamination of Tl (Karbowska, 2016).

In spite of its acute toxicity, very little is known about the chemical speciation of thallium in mining-metallurgical by-products and wastes which hampers the design and development of remediation and assisted attenuation techniques for Tl-polluted areas. In this regard, whereas total Tl concentration is a significant measurement index of the geochemical behavior and environmental hazard posed by this element, the transport properties, mobility and toxicity mostly depend on its geochemical fractionation (Ure et al., 1993; Bacon and Davidson, 2008; Rao et al., 2008). This partitioning can be determined by a sequential extraction procedure in order to obtain different fractions (soluble, exchangeable, reducible, oxidizable) by using suitable extractants. In addition to these labile fractions, Tl entrapped in the residual fraction also provides valuable information regarding the amount of element that is environmentally inaccessible (Sahuquillo et al., 2003).

To our knowledge, only a few research studies have been carried out concerning Tl fractionation in environmental scenarios, and there are still many unknown factors and conditions influencing the behavior of Tl during the mining and smelting processes of Tl-bearing ore materials. Most of these studies focused on contaminated soils and sediments in Poland, Spain, and China to predict mobility and bioavailability of Tl (Lis et al., 2003; Jia et al., 2013; Gomez-Gonzalez et al., 2015b; Vaněk et al., 2015; Liu et al., 2017a; b; Lukaszewski et al., 2018), and only one has ever been reported in Mexico (Cruz-Hernández et al., 2018). However, very little has been done about partitioning studies in potentially contaminating sources of Tl, which may become important for pollution control strategies, such as those carried out in Zn–Pb ores (Karbowska et al., 2014; Liu et al., 2016), Fe–Ni metallurgical slag and wastes from gold mineralization areas (Paldyna et al., 2013), fly ashes from burning of hard coal in stocker-fired boilers (Swietlik et al., 2016), and pyrite ores and slag from sulfuric acid plants (Yang et al., 2009).

The distribution, mobilization, and fate of Tl from mining-metallurgical contamination sources in Mexico have never been an environmental concern despite the fact that Mexico hosts one of the largest Pb–Zn ore deposits in the world (Clark and Fitch, 2009). This is especially relevant considering that mining and manufacturing of similar polymetallic deposits are responsible for most of the Tl dissemination into the environment (Xiao et al., 2004; Belzile and Chen, 2017). One reason of this lack of information about Tl distribution in ore processing plants could be related to the fact that individual mines often do not want their Tl concentration published, as indicated by Peter and Viraraghavan (2005). We carried out preliminary analyses of waste dump leachates from a Pb–Zn–Cu ore processing plant in the Cerro de San Pedro mining district (San Luis Potosí, Mexico). They confirmed the occurrence of Tl in concentrations (total and labile) several orders of magnitude higher than USEPA's drinking water (2 μg L^{-1}) and wastewaters (140 μg L^{-1}) guidelines (USEPA, 2016).

The purpose of this work, therefore, is to correctly define the potential risk associated with the presence of Tl in ores, by-products and wastes originated from different mining-metallurgical activities. The main goals of this study were: (1) to identify any possible Tl-bearing deposits in Mexico; (2) to investigate those mining-metallurgical products, by-products and/or wastes containing total Tl concentration above 1 mg kg^{-1}; (3) to delve into chemical speciation, distribution and potential mobility of Tl in these solid phases as determined by a sequential extraction procedure; and (4) to assess the impact caused by Tl mobilization on nearby stream sediments. To achieve these goals, wet chemical analyses were coupled with XRF, XRD, and SEM characterizations.

2. Materials and methods

2.1. Sampling

More than 60 samples of both crude and processed ores were taken from various epithermal polymetallic deposits in Mexico (Fig. 1). The samples were collected in triplicate and correspond to different stages of the processing and manufacturing of Zn–Pb–Cu and Ag–Au mineral deposits, including products such as crude ore, pre- and post-flotation by-products, ore concentrates, tailings, fly ashes, and wastes. Among these, and according to the Tl content (Table 1), six samples were selected for in-depth research: three from different Au–Ag post-flotation processes (M4, M22, and M36), a fly ash from a Zn–Pb ore roasting process (M28), a Cd-rich by-product from a Zn–Pb–Cu ore deposit (M45), and one belonging to a waste rock pile (M46) from a Zn–Pb–Cu ore deposit in the Cerro de San Pedro (CSP) mining district. In addition, two streambed sediments samples (M47-M48, 0–5 cm depth) were taken just below the waste pile (M46) to estimate the impact of intermittent leaching on the sediment surface (Fig. 2). Due to a non-disclosure agreement, we are not able to publicly reveal more details than those included here about the processing and smelting plants nor to divulge the names of the companies.

2.2. Sample preparation and digestion procedure

In all cases, samples were transferred to the laboratory in plastic zipper bags, crushed, air-dried for several days, ground to a powder in agate mortar (<45 μm grain size), and homogenized prior to chemical analysis. To determine the presence and concentration of thallium in the collected samples, a pseudo-total extraction procedure was performed by acid digestion with *aqua regia*. The use of hydrofluoric acid (HF) digestion step was omitted as *aqua regia*

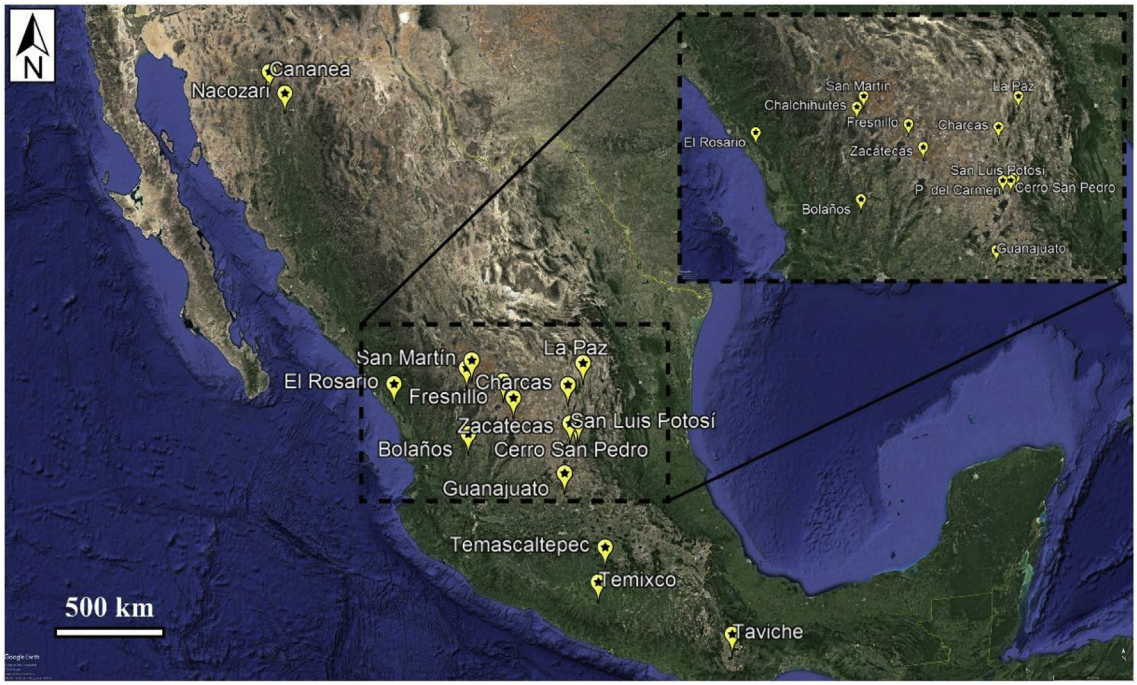

Fig. 1. Google Earth satellite image showing the location of samples taken from different mining districts in Mexico.

digestion is considered adequate enough in environmental studies as it aims to investigate the amount of metals and metalloids that can be released under common environmental conditions of pressure, temperature and pH (Rieuwerts et al., 2014). Briefly, 10 mL of a 3:1 mixture of concentrated HCl:HNO_3 solution were added to an aliquot of 0.5 g of each sample in a Teflon vessel and digested in a microwave oven (CEM-Mars X) at 120 °C for 30 min. The obtained acidified solutions were then filtered through Whatman No. 42 filter papers, brought to 50 mL with ultra-pure water (18.2 MΩ) and stored at 4 °C before they were analyzed for Tl by inductively coupled plasma-mass spectroscopy (ICP-MS). Montana Soil SRM 2710 (SRM, 2003) from the National Institute of Standards and Technology (NIST, USA) was used as standard reference material for quality control. All digestion experiments were carried out in triplicate.

2.3. Sequential extraction procedure

A key factor of the potential toxic effect of Tl in by-products and wastes from mining-metallurgical activities is Tl mobility. For this purpose, those samples with Tl concentration above 10 mg kg^{-1} determined by *aqua-regia* digestion were selected for further sequential extraction procedure. The selected samples were then subjected to a modified four-step sequential chemical extraction scheme (Table S1) proposed by the Community Bureau of Reference (Ure et al., 1993) with an additional intermediate step based on Caraballo et al. (2009). The modification of the original BCR method relies on the fractionation of total Tl bound to crystalline and poorly-crystalline reducible phases, which is not considered in the original BCR method. The partitioning procedure employed in this study comprised the following fractions: (F1) extracted with 0.11 M acetic acid that corresponds to the exchangeable/acid-extractable fraction; (F2) extracted with 0.5 M hydroxylamine hydrochloride at room temperature to mainly target poorly-crystalline Fe and Mn oxyhydroxides and oxyhydroxisulfates; (F3) extracted with 0.2 M ammonium oxalate (90 °C) to mainly target crystalline Fe and Mn minerals; and (F4) extracted with 30% hydrogen peroxide and 1 M ammonium acetate, that corresponds to organic matter or oxidizable phases (sulfides). The residual fraction (*s.l.*) of Tl was calculated as the difference between the pseudo-total concentration of Tl extracted with *aqua regia* digestion and the sum of Tl concentrations in the four fractions (F1+F2+F3+F4). After each solid-solution interaction, the resulting suspensions were centrifuged at 3000 rpm for 15 min and filtered through a 0.45 μm PVDF membrane syringe filter. The supernatant was then transferred to polyethylene tubes, acidified with HNO_3, and stored at 4 °C prior to determination of Tl concentration by ICP-MS. The solid residue was washed twice with 10 mL of ultra-pure water (18.2 MΩ) before using it for the subsequent step.

Analytical quality assessment was also carried out on the basis of the certified reference material (CRM) Montana Soil SRM 2710.

3. Results and discussion

3.1. Total thallium content

Forty-eight (48) out of the 63 samples collected from different mining–metallurgical sites showed Tl concentrations above 0.01 mg kg^{-1} (Table 1). It is important to emphasize that these values were obtained from acid digestion with *aqua regia* and, as we mentioned above, represent an accurate amount of element to be potentially released under natural conditions (Escarré et al., 2011; Anagboso et al., 2013; Rieuwerts et al., 2014). Montana soil 2710 (NIST) was also analyzed following the same digestion procedure as described for the samples, resulting in a Tl concentration value of 0.71 mg kg^{-1}, within the certified concentration range (Table 1). This analysis confirmed the validity of microwave-assisted digestion and ICP-MS determination methods employed for the mining-metallurgical and sediment samples.

Crude ores, concentrates, by-products and, particularly, wastes from mining-metallurgical sites analyzed in this study are highly enriched in Tl compared to the average crustal abundance of

Table 1
Average (n = 3) thallium content (mg kg^{-1}) in samples collected from mining-metallurgical activities in different mining zones of Mexico determined by ICP–MS.

Code[a]	Sample	Thallium concentration[b]
M1	Au–Ag-rich ore (Guanajuato)	0.41
M2	Au–Ag ore concentrate (Guanajuato)	1.64-1.70
M3	Au–Ag-rich ore tailing (Guanajuato)	0.28
M4†	Ag-rich ore (Zacatecas)	12.6
M5	Ag-rich ore (Baja California)	0.50–0.57
M6	Cu-rich ore (San Luis Potosí)	0.46–0.53
M7	Ag ore concentrate from Cu deposits (San Luis Potosí)	2.33–2.42
M8	Ag ore from As–Sb–Pb deposits (Michoacán)	5.39
M9	1st flotation of Cu (Zacatecas)	0.29
M10	2nd flotation of Cu (Zacatecas)	0.32
M11	3rd flotation of Cu (Zacatecas)	0.43
M12	Cu ore concentrate (Zacatecas)	0.95–1.03
M13	Cu ore tailing (Zacatecas)	0.14–0.20
M14	Pb–Ag ore concentrate (Jalisco)	0.62
M15	Zn–Ag ore concentrate (Jalisco)	0.89
M16	Sulfides and oxides from Pb–Zn–Ag ore (Jalisco)	0.50
M17	Pb–Zn–Cu-rich ore (Oaxaca)	0.57
M18	Cu ore concentrate (Oaxaca)	4.31
M19	Pb ore concentrate (Oaxaca)	5.20
M20	Zn ore concentrate (Oaxaca)	1.10
M21	Pb–Zn–Cu-rich ore tailing (Oaxaca)	0.30
M22†	Oxides from Au–Ag ore (Morelos)	45.6
M23	Zn–Pb–Ag-rich ore (Zacatecas)	1.42–3.74
M24	Molybdenite from Cu deposits (Sonora)	1.12–3.23
M25	Zn–Pb–Cu–Au-rich ore (San Luis Potosí)	0.13
M26	Zn–Pb–Cu–Au-rich ore tailing (San Luis Potosí)	0.08
M27	Dumps of Zn–Pb ore (San Luis Potosí)	1.47
M28†	Fly ash from Zn–Pb ore (San Luis Potosí)	49.6
M29	Fly ash from Zn-rich ore (San Luis Potosí)	1.82
M30	Oxides from Pb–Zn–Cu–Ag deposits (Zacatecas)	0.40–0.52
M31	Sulfides from Pb–Zn–Cu–Ag deposits (Zacatecas)	0.74–1.92
M32	Pb ore concentrate (Zacatecas)	3.32
M33	Zn ore concentrate (Zacatecas)	0.82
M34	As ore from Pb–Zn–Cu–Ag deposits (Zacatecas)	1.71–3.30
M35	Au–Ag-rich ore (Estado de México)	11.1
M36†	Au–Ag ore concentrate (Estado de México)	78.5
M37	Au–Ag-rich ore tailing (Estado de México)	5.43
M38	Pb–Zn–Ag-rich ore (Zacatecas)	0.47
M39	Ag ore concentrate (Zacatecas)	1.18
M40	Pb–Zn–Ag-rich ore tailing (Zacatecas)	0.29
M41	Zn ore concentrate from Cu–Zn deposits (San Luis Potosí)	1.26
M42	Jarosite-rich waste from Cu–Zn smelting tailing (San Luis Potosí)	7.29
M43	Dust from Cu–Zn ore (San Luis Potosí)	1.71
M44	Refined Cu-rich by-product (San Luis Potosí)	9.96
M45†	Refined Cd-rich by-product (San Luis Potosí)	169.8
M46†	Waste pile from Zn–Pb–Cu ore (CSP, San Luis Potosí)	199.7
M47†	Stream sediment (Zn–Pb processing area, CSP, San Luis Potosí)	5.45
M48†	Stream sediment (Zn–Pb processing area, CSP, San Luis Potosí)	5.90
	NIST 2710[c]	0.71 (0.50–0.76)

[a] Codes followed by (†) denote selected samples for in-depth research.
[b] Tl concentration was measured by ICP-MS after microwave-assisted digestion with *aqua regia*.
[c] In parenthesis, recovery range of SRM 2710 Montana soil as certified by the National Institute of Standards and Technology (NIST).

0.49–1 mg kg^{-1} (Peter and Viraraghavan, 2005; Kabata-Pendias, 2011). The Tl content values displayed in Table 1 vary depending on the mining district, type of ore, and processing step, and are in good agreement with comparable samples from other Tl-bearing deposits in the world like those reported in Poland (Lis et al., 2003; Karbowska et al., 2014), Spain (Alastuey et al., 1999; Gomez-Gonzalez et al., 2015b; Lopez-Arce et al., 2017), and China (Yang et al., 2009; Xiao et al., 2012; Liu et al., 2016). Overall, ore concentrates have higher pseudo-total Tl content than raw ore samples and tailings, as can be seen in samples M1 to M3, M17 to M21, and M35 to M37 from Guanajuato, Oaxaca and Estado de México mining zones, respectively. This supports the fact that Tl content generally increases during flotation processes (Liu et al., 2016) and it agrees with Tl content distributions among the crude and processed ore concentrates described by Karbowska et al. (2014) and Liu et al. (2016). In addition, results shown in Table 1 also highlight the presence of Tl in polymetallic sulfide deposits accompanying metals and metalloids such as Zn, Cu, Pb, Ag, Sb, or As due to its geochemical chalcophile properties (Peter and Viraraghavan, 2005). For instance, high Tl concentrations have been observed in pyrite and cinnabar (24.7 and 152 mg kg^{-1}, respectively) from Hg deposits in Guangxi, China (Xiao et al., 2012); in galena, sphalerite and pyrite (1.2, 1.6 and 9.2 mg kg^{-1}, respectively) from Sb deposits in Hunan, China (Zhou et al., 2011); or in blende and galena (10.1 and 7.3 mg kg^{-1}, respectively) from Zn–Pb deposits in Poland (Karbowska et al., 2014).

In general, soil Tl contents above 1 mg kg^{-1} indicate pollution and this concentration is proposed as the maximum allowable concentration (MAC) value for environmental solid samples (Kabata-Pendias, 2011). In our case, 28 out of 48 samples showed Tl

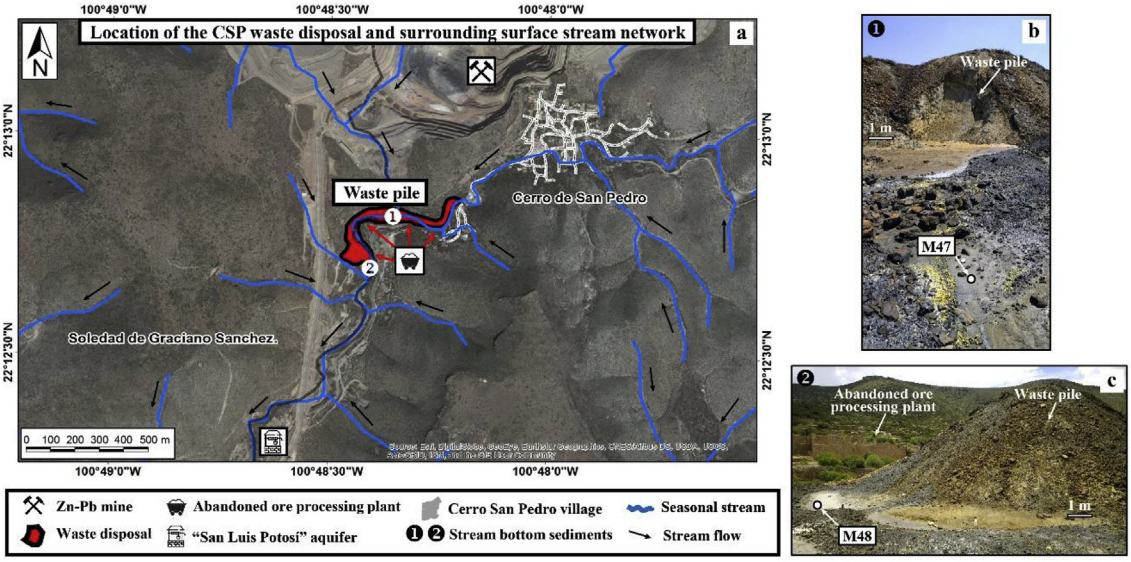

Fig. 2. DigitalGlobe map of the Cerro de San Pedro (CSP) studied area (a), showing the sample locations of the waste pile and streambed sediments (b–c) from an abandoned ore processing area in San Luis Potosí, Mexico.

content above the MAC value, including the two stream sediments from the Zn–Pb processing area in the CSP historical mining district (M47-48, Table 1, Fig. 2). By-products and residues obtained during Zn–Pb–Cu ore processing contain higher amounts of Tl than those from Au–Ag-rich ores. In fact, the sample with the highest Tl content is the one collected from the Zn–Pb waste pile in CSP (M46, 199.7 mg kg^{-1}) followed by the by-product collected from a Cu–Zn smelting plant (M45, 169.8 mg kg^{-1}). Although the major sources of Tl are sulfide ores, it can also be found associated with oxy-hydroxides after the oxidation of Tl-bearing Fe sulfides (Kazantzis, 2000; Vaněk et al., 2013; Gomez-Gonzalez et al., 2015b; Lopez-Arce et al., 2017). This is the case of sample M22 from an Au–Ag ore in Temixco, Morelos (Table 1, Fig. 1), where high amounts of Tl were bound to iron oxyhydroxides, as discussed below.

The fractions obtained during roasting/smelting of Tl-hosting sulfides such as slags, ashes or dusts, may contain significant amounts of Tl due to the low melting and boiling point of the element, which promotes its volatility (Nriagu, 1998; Liu et al., 2016). When Tl-rich sulfide minerals are exposed to high temperatures (900–1200 °C), Tl may mobilize from the ore and it is converted into the gaseous form (volatilized). Subsequently, it enters the furnace flue or chimney, and it is then partially condensed on the low-temperature surface areas of the ash particles. This can be attributed to the surface structure of the ash components, as the gaseous Tl produced during ore roasting is more easily adsorbed by these small, poorly-crystalline particles, which usually provide more adsorption sites. The longer the contact time between the ash and exhaust fumes, the higher the concentration of Tl in ash, which could be orders of magnitude higher compared to prior to roasting (Karbowska, 2016; Liu et al., 2016). In this work, sample M28 is a good example of this phenomenon as the fly ash from the Zn–Pb ore roasting process is strongly enriched in Tl (49.6 mg kg^{-1}, Table 1) compared to the crude ore (0.13 mg kg^{-1}) (M25, Table 1). Thallium partitioning between the slag, fly ash, and flue gas mainly depends on its mode of occurrence in the raw and processed materials, as well as the conversion technology of the smelting and refining plant. Operational parameters such as fuel preparation, burning process, size of minerals and physicochemical properties of Tl-containing phases are other factors that influence Tl volatilization (Folgueras et al., 2017). Similar Tl behavior has also been observed in other industrial activities involving sulfide roasting processes, i.e. cement or sulfuric acid production, as well as coal-fired power plants, since most coals contain about 0.11–135 mg kg^{-1} of Tl incorporated in sulfides (Cheam, 2001; Anton et al., 2013; Chen et al., 2013). Due to the weak sorption mechanism of Tl in these scenarios (mostly adsorption), Tl mobilization from industrial ashes and dusts may lead to hazardous Tl pollution. For instance, WHO/IPCS (1996)) stated that Tl from dusts was more available to be absorbed by plants than Tl in soil from a Pb–Zn mining area. Therefore, a careful control of these materials is required to prevent Tl solubilization and mobilization into the environment.

The amount of Tl found in the sediments, 5.45–5.90 mg kg^{-1} (M47-48, Table 1), is one order of magnitude higher than the median Tl content of 0.39 mg kg^{-1} (n = 848) calculated from contaminated and uncontaminated European stream sediments according to FOREGS data produced by the EuroGeoSurvey (Salminen, 2005), the most comprehensive source of information to date in this regard. In general, the distribution of Tl in stream sediments is essentially natural, related to felsic or granitic geological associations. However, Tl stream sediment anomalies compiled in the FOREGS database are the result of contamination by mining and smelting activities, typically associated with Zn–Pb ore deposits. Lis et al. (2003) also noted that Zn–Pb ores exploitation leads to a significant increase of Tl concentration in the top layer of soil and stream sediments. This matches the observed processes in the studied area (CSP), where the streambed sediments collect runoff originating from the mining wastes (Fig. 2b and c). The Tl content found in both M47 and M48 sediment samples is similar to those concentrations reported by Jakubowska et al. (2007) and Karbowska et al. (2014) in rivulet (6.6 mg kg^{-1}) and stream (7.5 mg kg^{-1}) sediments close to the Trzebionka Zn–Pb ore mine in Poland. High concentrations of Tl in stream sediments constitute a direct threat to the environment due to possible leaching into underground waters, downstream mobilization, and uptake by plant roots with consequent accumulation in plant biomass. As a result, Tl may enter the food chain and be stored in living organisms causing harmful health effects (Kazantzis, 2000; Peter and Viraraghavan, 2005; Karbowska, 2016). In addition, the Tl concentration gap between the waste pile (199.7 mg kg^{-1}, M46,

Table 1) and the impacted sediments (5.45–5.90 mg kg^{-1}, M47-48, Table 1) indicates that most of the leached Tl is not accumulated in the sediments, but dispersed. This could be related to the solubility degree of Tl from the waste pile and/or to a possible dispersion of Tl through association with environmental vectors, that is, colloidal particles capable of transporting metals and metalloids in solid-water systems (Hamon et al., 2005; Gomez-Gonzalez et al., 2018). This may have important implications for the potential bioavailability of Tl (and other PTEs associated), as well as for water usage for human consumption.

3.2. Chemical and mineral composition

Samples with Tl content above 10 mg kg^{-1} (10-times the MAC value) were selected for further analyses, with the exception of sample M35 due to its similarity to sample M4 (Table 1). Additionally, the streambed sediments were also selected due to their environmental significance. The elemental composition along with the principal mineral phases of selected samples are shown in Table 2, and Table 3 and Fig S2 respectively. Montana soils 2710a and 2711a (NIST) and the ore reference material OREAS 111b were subjected to the same procedure as described for the samples, resulting in similar concentration values for selected elements than the certified ones (Table 2).

The results indicate that the solid phases contain relatively high amounts of Pb, Zn, Cu, and Fe sulfides and sulfates, but low quantities of other minor and trace elements such as Cd, As, Sb, or Mn, depending on the ore deposit and processing step. All samples show loss of S characteristic of sulfur depletion during ore processing as sulfide minerals undergo strong oxidation, which invokes sulfur release converted to SO_2 gas. In general, Tl-enriched samples with higher amounts of Ag (M22, M36) contain lower amounts of Zn, Pb, Cu, and Cd than those where Ag is negligible. This may be due to the type of sample, as Ag-rich samples are ore concentrates obtained from a post-flotation process while Ag-poor samples are by-products and wastes derived from Zn–Pb ores. As a consequence, the different steps involved in the ore processing affected the mineralogical composition of the samples. For instance, the main crystalline minerals observed in sample M22 are quartz and jarosite ($KFe_3(SO_4)_2(OH)_6$), whereas mineral cernyite (Cu_2CdSnS_4) has only been detected in sample M36 (Table 3), whereas X-ray diffraction patterns of samples M28, M45, and M46 show a myriad of peaks as a result of a greater transformation process of the ore (Fig. S1). In the case of sample M28, chlorides and bromides were the main mineral phases. This was further confirmed by SEM-EDS microscopy analysis in which multiphase particles with Cu, Pb, Zn, Cl, and Br as major components were observed (see section 3.3). The elemental composition of the ash agrees with samples (dusts) of other Pb–Zn smelting processes (Liu et al., 2016, Fig. 4 therein).

Pearson's correlation coefficient (r) was calculated to study whether there is any relationship between the pseudo-total concentration of Tl and the concentration of other elements in these samples. In general, Tl content did not show a significant correlation with any other element. However, we found a positive correlation between the concentrations Tl and Mn ($r = 0.79$, $R^2 = 0.54$) as well as S ($r = 0.81$, $R^2 = 0.57$), showing a certain affinity between these elements (Table 2). This suggests that Tl may be associated with Mn- and/or S-rich mineral phases by different sorption mechanisms, most likely structural incorporation or surface adsorption (Lis et al., 2003; Gomez-Gonzalez et al., 2015a; Liu et al., 2016; Aguilar-Carrillo and Herrera-García, 2018; Cruz-Hernández et al., 2018), and the formation of several Mn- and S-rich mineral phases also supports this correlation (Table 3).

Although in some cases a low S content can be taken as a low contamination risk, wastes with low-sulfur content (S < 3 wt%) can locally be an important source of acid mine drainage (AMD) and may have severe environmental impacts on their surroundings (Parviainen et al., 2012). This is especially relevant in the CSP mining district where both a Zn–Pb waste pile (M46) and streambed sediments (M47-48) are located (Fig. 2). Despite the low-sulfur content of the waste pile (~5 wt%), the nearby sediments are enriched in Fe and S, and accumulate significant amounts of pollutants such as Pb, Zn, As, and Tl, released by continuous weathering of the waste pile (Table 2). The sediments contain higher concentrations of elements than the waste (except Zn and Mn), with Fe and S as the main components. X-ray diffraction analysis showed jarosite and gypsum ($CaSO_4 \cdot 2H_2O$) as the main crystalline minerals within the sediment samples M47-48 (Table 3). These two phases were already observed in the waste pile sample

Table 2
Average (n = 3) element concentration of selected samples according to ore deposit and mineral processing method applied determined by XRF.

Sample	Tl[a]	Au	Ag	Pb	Cu	Zn	Cd	Fe	As	Sb	Mn	S
	mg kg^{-1}			wt%								
Ores and wastes												
M4	12.6	BDL[c]	178	1.02	0.12	1.22	0.038	0.73	BDL	0.06	0.01	0.35
M22	45.6	9.84	1480	3.71	0.14	0.17	BDL	21.7	0.58	0.24	0.03	2.06
M28	49.6	27.4	BDL	13.4	9.29	6.95	0.23	0.29	0.21	0.082	0.03	2.04
M36	78.5	97.7	4610	0.82	0.18	1.85	0.015	12.8	0.46	0.12	0.04	4.06
M45	169.8	BDL	BDL	0.76	5.48	45.9	18.9	0.09	0.01	4.46	0.11	2.96
M46	199.7	BDL	BDL	0.073	0.013	2.61	0.010	12.8	0.041	0.007	0.61	5.14
Sediments												
M47	5.45	BDL	BDL	0.53	0.022	0.31	BDL	20.9	0.397	0.010	0.041	3.30
M48	5.95	BDL	BDL	0.74	0.023	0.80	0.008	13.7	0.135	0.012	0.014	3.15
Reference materials[b]												
NIST 2710a	BDL	BDL	36	0.56	0.37	0.41	BDL	4.83	0.15	BDL	0.18	0.87
NIST 2710a values	1.52 ± 0.2	0.2	40	0.55 ± 0.00	0.34 ± 0.01	0.42 ± 0.00	12.3 ± 0.3	4.32 ± 0.08	0.15 ± 0.00	0.01 ± 0.00	0.21 ± 0.01	n.r
NIST 2711a	BDL	BDL	BDL	0.130	0.01	0.034	0.004	2.62	0.01	BDL	0.06	0.051
NIST 2711a values	3	n.r.	6	0.14 ± 0.00	0.01 ± 0.00	0.04 ± 0.00	0.005 ± 0.00	2.82 ± 0.04	0.01 ± 0.00	0.002 ± 0.00	0.07 ± 0.00	n.r.
OREAS 111b	BDL	BDL	BDL	0.04	2.23	0.40	BDL	31.9	0.02	BDL	BDL	14.9
OREAS 111b values	n.r.	n.r.	<20	0.04 ± 0.00	2.44 ± 0.13	0.43 ± 0.02	0.002 ± 0.00	35.5 ± 1.8	0.02 ± 0.00	0.002 ± 0.00	n.r.	n.r

nr., not reported.
[a] Tl concentration measured by ICP-MS after microwave-assisted pseudo-total digestion and included here for the sake of comparison.
[b] Reference certified and non-certified concentration values in mg kg^{-1} and wt% with relative standard deviations of selected certified materials.
[c] Below detection limit.

Table 3
Main mineral phases of selected samples as determined by XRD analysis.

Sample	Phases[a]	Undiffracted fraction (wt%)
M4	Quartz (Q), Cr-Zn sulfide (ZnS^{Cr})	19.1
M22	Quartz (Q), Plumbojarosite (Pb-Jr)	19.6
M28	Cu(OH)Cl (Cc), PbBrCl (Lbc); $Pb_3O_2(SO_4)$ (Lo)	20.0
M36	Quartz (Q), Cernyite (Cn)	10.3
M45	Lavendulan (Lv), Parabutlerite (pbt), $Cu_3(AsO_4)_2$ (CuAs), Szmikite (Sz), Franklinite (Fk)	19.3
M46	Quartz (Q), Jarosite (Jr), Birnessite (Bn), Bassanite (Bs), $MnO \cdot H_2O$ (MnO), Cd–Zn-rich Zeolite (Zt), Gypsum (G)	17.7
M47	Quartz (Q), Gypsum (G), Jarosite (Jr), $PbHAsO_4$ (La), Kaolinite (K)	14.7
M48	Quartz (Q), Gypsum (G), Jarosite (Jr), Sulfur (S)	13.2

[a] The X-ray diffractogram of each sample can be found in Fig. S1 of the ESI file.

(M46), suggesting that mineral phases in the streambed sediments are, somehow, inherited from the waste material. In other words, weathering of the waste pile triggers the oxidation and/or solubilization of sulfides and other phases present in the sample (Table 3), releasing the oxidized ions Fe(II)/Fe(III), S(VI), As(III)/As(V), Mn(II)/Mn(IV), among others, and promoting the formation of fresh secondary minerals that can reach the sediments below. The presence of poorly-crystalline phases like Fe/Mn oxyhydroxides as well as amorphous ferric arsenate (AFA) in the streambed sediments cannot be ignored, as approximately 13–15% of the solid phase corresponds to an amorphous fraction according to the crystallinity degree estimated by semi-quantitative XRD analysis. The occurrence of both crystalline and poorly-crystalline Fe/Mn phases in soils and sediments impacted by mining-metallurgical wastes is widely known and play an important role in PTEs immobilization (Blowes et al., 2003). The amount of Tl abruptly decreased in sediments compared to the neighboring waste pile (Table 2). This could be explained by several factors as (i) the progressive depletion of sulfides in the oxidized surface wastes, (ii) attenuating mechanisms such as Tl adsorption and transport by newly-formed secondary minerals, (iii) and most likely increasing surface runoff of the contaminant plume that could eventually reach groundwater system by percolation. Along with Tl depletion, it is also relevant that crystalline Mn phases are not detected in the sediments despite being observed in the waste pile (Table 3), with Mn concentration in the former being one order of magnitude lower than in the latter (Table 2). This may be related to the transformation of Mn phases at pH values of the leachates from the waste (1.9–2.3), with most of the Mn solubilized and mobilized instead of re-precipitated in the sediment (Tu et al., 1994). Thus, the weathering of the waste pile very likely lead to the formation of Mn-rich colloids, which are ubiquitous particles that can be efficiently transported. Consequently, Mn colloidal phases can act as geochemical vectors (carriers) for Tl transport in the waste-sediment-stream system, playing a pivotal role in Tl mobilization (Lis et al., 2003).

3.3. Modified BCR sequential extraction

The amount of Tl in each geochemical fraction from the modified BCR sequential extractions of the investigated samples, as well as in the SRM 2710 reference material, are shown in Table 4. Although SRM 2710 is only certified for total Tl content, it can be useful for evaluating the Tl extractability. Results from Tl fractionation in reference materials processed in similar sequential extraction procedures have been previously reported by Gomez-Gonzalez et al. (2015b) and Liu et al. (2016). In addition, for a better comparison of the potential mobilization of Tl among the samples, the absolute amounts of Tl in each fraction are also displayed in Fig. 3. Labile fractions of Tl were computed as the sum of the concentrations measured in F1–F4. As it was described by Bacon and Davidson (2008) and Anagboso et al. (2013), the associations of Tl presented here are operational and although specific mineral phases are targeted, results strictly reflect the solubility of Tl in particular reagents under particular conditions.

Thallium in Ag–Au ore concentrates, M4 and M36, was mostly found in the residual fraction (78 and 55%), followed by the oxidizable (16 and 13%) and crystalline reducible fractions (3 and 22%, respectively) (Table 4, Fig. 3). However, little amounts of Tl were found in both exchangeable (1.7–2.3%) and poorly-crystalline reducible (1.8–7.3%) fractions (F1 and F2, respectively). The presence of Tl in the residual fraction is related to Tl bound to aluminosilicates and other well-crystallized minerals, e.g., quartz, feldspars, or mica, whereas that in the oxidizable fraction is targeting mainly sulfides (e.g., ZnS, Cu_2CdSnS_4) as it was observed by XRD (Table 3). These solid phases were also observed with the SEM-EDS in the form of particles of metallic alumino-silicates and sulfides (Fig. S2,a-d). It has also long been suspected that the presence of Tl in the residual fraction of samples derived from mining-metallurgical activities may reflect the existence of Tl in refractory matrices formed during the ore processing (Anagboso et al., 2013). From an environmental perspective, Tl attached to the residual fraction indicates low extractability under natural conditions. Thus, the amount of Tl in this fraction is practically unavailable in comparison to labile fractions (Bacon and Davidson, 2008; Lukaszewski et al., 2018).

In contrast, the Tl in samples obtained after roasting (M28) and refining (M45) processes was mostly found in the acid exchangeable (58 and 63%) and poorly-crystalline fractions (26 and 28%, respectively) (Table 4, Fig. 3), suggesting preferential affinities of Tl towards surface adsorption sites and amorphous phases. High-temperature roasting and smelting processes can activate and mobilize significant amounts of Tl due to partial oxidation of sulfides. Accordingly, Tl is released and transformed into gaseous forms during the roasting of the ore concentrate, and then deposited onto ash particles through weak sorption mechanisms such as physicochemical adsorption or condensation reactions (Liu et al., 2016).

The mineralogy of samples M28 and M45 are displayed in Table 3. Metallic oxides and sulfates are the dominant crystalline phases in sample M45, whereas metallic halides predominate in sample M28. In addition, XRD analysis revealed that both M28 and M45 samples contain an amorphous fraction of approximately 20% each. This would explain the high amounts of Tl found in fraction F2 in these samples (Table 4), supporting that Tl is also bound to poorly-crystalline phases (Martín et al., 2004; Lopez-Arce et al., 2017). The formation of amorphous particles that may (re)adsorb Tl was observed by SEM in both samples (Fig. S2,e-h). The occurrence of halides (F, Cl, Br) in Pb–Zn ores is very common (Ackermann et al., 1999) and they can play an important role in Tl volatilization due to the formation of stable Tl halides, along with oxides, under strong oxidation conditions (Liu et al., 2016). Despite the fact that none of these Tl halide compounds were found during

Table 4
Average (n = 3) solid-phase distribution of thallium (mg kg^{-1}) in ores, wastes, and sediments determined by the modified BCR sequential extraction procedure.[a]

Sample	F1		F2		F3		F4		Labile Tl[d]		Residual[e]		Total[f]
	Tl[b]	%[c]	Tl	%	Tl	%	Tl	%	Tl	%	Tl	%	Tl
M4	0.21	1.67	0.23	1.83	0.40	3.17	1.98	15.8	2.82	22.4	9.78	77.6	12.6
M22	1.12	2.46	14.1	31.0	22.2	48.8	1.74	3.82	39.2	86.0	6.4	14.0	45.6
M28	28.5	57.5	12.8	25.8	11.9	24.0	3.39	6.83	56.6	114.1	n.a.	n.a.	49.6
M36	1.84	2.34	5.76	7.31	17.2	21.8	10.6	13.4	32.0	44.9	46.8	55.1	78.8
M45	107.0	63.2	47.5	28.1	13.8	8.14	7.85	4.64	176.1	104.0	n.a.	n.a.	169.8
M46	72.5	36.3	80.4	40.3	26.0	13.0	5.46	2.73	184.4	92.3	15.3	7.67	199.7
M47	0.30	5.53	0.87	16.0	1.61	29.5	0.22	3.98	3.00	55.0	2.45	45.0	5.45
M48	0.13	2.20	0.29	4.90	1.43	24.0	0.18	2.97	3.92	34.1	2.03	65.9	5.95
SRM 2710	0.07	9.3	0.16	22.6	0.40	55.8	<0.01	n.a.	0.63	87.7	0.087	12.3	0.71

n.a., not applicable.
[a] The modified BCR procedure is described in Section 2.3 and Table S1.
[b] Mean value of extracted Tl in the corresponding modified BCR step calculated by ICP-MS.
[c] .Percentage of extracted Tl of each fraction as compared to the pseudo-total measurement determined by ICP-MS (Table 1).
[d] Extracted Tl as the sum of the modified BCR steps (F1+F2+F3+F4).
[e] Residual = Pseudo-total − Sum (F1+F2+F3+F4).
[f] Pseudo-total concentration of Tl in samples determined by ICP-MS after acid digestion with *aqua regia* (Table 1).

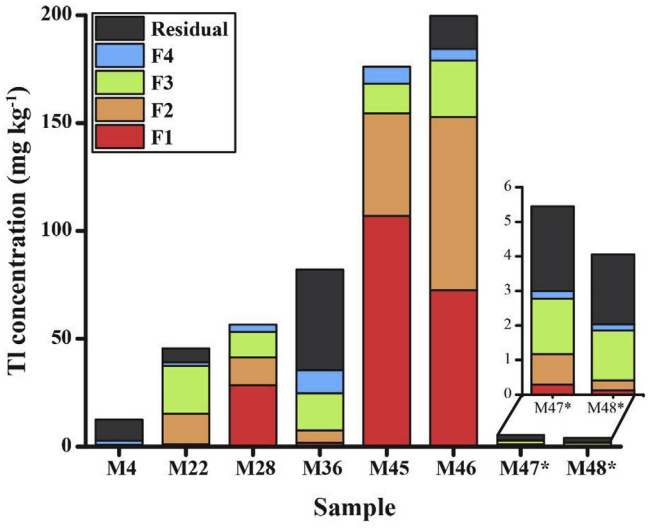

Fig. 3. Absolute concentrations of Tl (mg kg^{-1}) distributed among the geochemical fractions of selected samples determined by the modified BCR sequential extraction procedure. The inset shows details of Tl fractionation in both streambed sediments.

XRD analysis, relatively high amounts of Cl and Br were indeed observed by SEM-EDS as micron-size irregular ash particles (Fig. S2,e-f). This suggests that halides may have helped to the almost complete volatilization of Tl by forming gaseous Tl halides. The condensation, settling, or adsorption of these compounds onto the ash particles involve weak bonding between Tl halides and the particle's surface. This would explain why Tl is mostly extracted in the exchangeable F1 fraction (Table 4). Similar effects were also predicted by Anton et al. (2013) during coal combustion, where several gaseous Tl halides (TlBr, TlCl) may prevail at high temperatures. In any case, phase transformation during roasting process clearly increases the amount of Tl associated with fractions where Tl is more easily released (i.e., F1 and F2) (Lopez-Arce et al., 2017).

Regarding the M22 sample, minor amounts of Tl were extracted from the exchangeable fraction F1 (1.12 mg kg^{-1}, 2.5%, Table 4, Fig. 3). Thallium in this sample was mostly associated with poorly-crystalline F2 (14.1 mg kg^{-1}, 31%) and crystalline F3 (22.2 mg kg^{-1}, 49%) reducible fractions, likely metallic oxyhydroxides. This is in good agreement with the origin of the sample (oxides from the Au–Ag ore processing, Table 1) as well as with the average element composition determined by XRF in which Fe was the major element, followed by Pb (Table 2). Besides, X-ray diffraction analysis confirmed the presence of Pb-rich Fe-bearing phases such as plumbojarosite [$Pb_{0.5}Fe_3(SO_4)_2(OH)_6$] (Table 3). It is well known that jarosite-like compounds may incorporate PTEs into the mineral structure (Bayliss et al., 2010; Aguilar-Carrillo et al., 2018). In fact, Tl-bearing jarosite is an important secondary host phase for Tl (Dutrizac, 1997; Dutrizac et al., 2005; Voegelin et al., 2015), and its formation is suggested in this study for sample M42, in which a significant amount of Tl was found in jarosite-rich tailings (7.29 mg kg^{-1}, Table 1). Moreover, XRD analysis also revealed that M22 sample contains an amorphous fraction of approximately 20%, perhaps Fe-rich phases considering the amount of Fe in the sample (21.7 wt%, Table 2). This result, along with the large amounts of Tl extracted in the F2 fraction (14.1 mg kg^{-1}; 31%, Table 4), suggests that there is a connection between the Fe-rich poorly-crystalline phases and Tl (Lopez-Arce et al., 2017). This observation is in accord with those results obtained for M28 and M45 samples in which the high percentage of Tl was also found in the poorly-crystalline fraction F2 (Table 4). The presence of amorphous Fe oxyhydroxides in sample M22 was confirmed by SEM-EDS analysis (Fig. S2,i-j), along with agglomerates of tiny crystalline Fe-rich particles with high amounts of Pb and As (Fig. S2,k-l), presumably jarosite-like compounds, in which Tl may incorporate. Although some authors pointed out that Tl is not significantly sorbed to Fe minerals apart from Tl-jarosite (Jacobson et al., 2005; Smeaton et al., 2012; Coup and Swedlund, 2015; Voegelin et al., 2015), our results are in line with other studies where amorphous Fe (and Mn) oxyhydroxides generated due to mining-metallurgical activities may have an important role retaining Tl in impacted areas (Martín et al., 2004; Gomez-Gonzalez et al., 2015b; Lopez-Arce et al., 2017). Lastly, only small quantities of Tl were extracted from the oxidizable faction F4 (1.74 mg kg^{-1}, 3.8%, Table 4, Fig. 3), usually targeting organic matter and sulfide minerals. None of the phases identified by XRD in sample M22 were sulfides (Table 3), suggesting that most of the S is in the oxidized form [S(VI)], likely as SO_4^{2-} in the jarosite compounds. Therefore, the Tl extracted in fraction F4 may be bound to other oxidizable phases than sulfides or, at least, to sulfides that are not detected by either XRD or SEM-EDS analyses considering our detection limits (5 wt% and 1 wt%, respectively). Obviously, organic matter is not considered here due to the origin of the M22 sample.

From an environmental point of view sample M46, collected from the waste pile, is of great concern as it is situated at the

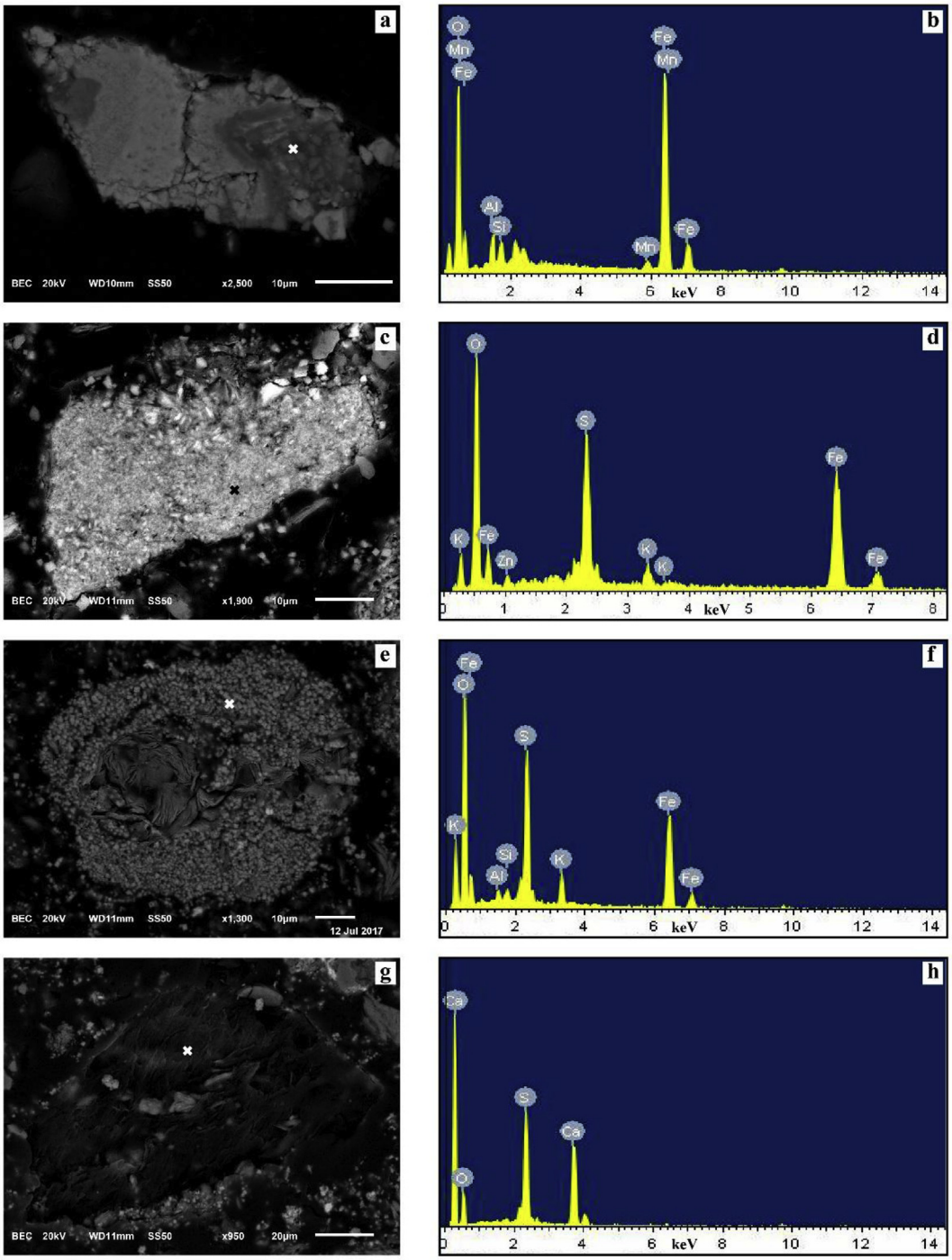

Fig. 4. Scanning electron microprobe (SEM) images and Energy Dispersive X-Ray Spectroscopy (EDS) analyses of selected sample M46; BEC: backscattered mode. (a–b) irregular Fe/Mn-rich oxide particle; (c–d) aggregation of Fe-rich sulfate nanoparticles; (e–f) micron-size crystals of jarosite; and (g–h) broken edges of layered calcium sulfate. Symbol (X) indicates location of EDS analysis.

confluence of seasonal streams that eventually feed the "San Luis Potosí" aquifer ($125.6 \cdot 10^6$ m^3/year) (Fig. 2), supplying water for both agricultural and domestic purposes. Besides, intense mining activities in the Cerro de San Pedro (CSP) historic mining district date back to 1870, and are still ongoing (Petersen et al., 2001; Studnicki-Gizbert and Schecter, 2010). This has resulted in the prolonged production and disposal of large amounts of waste in this site, where high levels of As, Pb, Cd, and Zn have been already reported in related samples (Vázquez, 2012). In addition, the highest Tl concentration determined in this work is found here (199.7 mg kg^{-1}, Table 1). Hence, Tl partitioning in the waste pile is crucial for further studies regarding mobilization and attenuation strategies. According to the sequential extractions of this sample (Table 4, Fig. 3), the greatest proportions occur in the poorly-crystalline reducible fraction F2 (80.4 mg kg^{-1}, 40%), closely followed by the exchangeable fraction F1 (72.5 mg kg^{-1}, 36%). In contrast, the amount of Tl in the residual fraction was comparatively low. Most of the studies focused on Tl partitioning in mining-

metallurgical wastes frequently report the residual fraction as the major reservoir of Tl, reaching values up to 89% in scorodite-rich mine wastes (Gomez-Gonzalez et al., 2015b) or even up to 97% in sphalerite-bearing mine wastes (Alvarez-Ayuso et al., 2013). In our case, however, results indicate that above 75% of Tl in the waste pile is bound to easily extractable or mobile fractions, indicating a fraction of Tl that is weakly bound to mineral surfaces. Only few amounts of Tl are associated with the less mobile fractions. Therefore, erosion and weathering process through the years clearly produced an enrichment of Tl in potentially mobile fractions where Tl is more easily released (F1, F2). Lis et al. (2003) reported that oxidation of sulfides from Zn–Pb waste dump to form sulfates increases the mobilization and dispersion of Tl. In this regard, we found different sulfate-based phases (i.e., jarosite, bassanite, gypsum) in sample M46 by XRD (Table 3). Some authors have described the formation of Tl-sulfate phases, such as lanmuchangite [TlAl(SO_4)$_2$·12H_2O], in areas with high levels of Tl and sulfate as a consequence of a high degree of sulfide oxidation (Chen et al., 2003; Xiong, 2009). Dorallcharite [(Tl,K)$Fe_3(SO_4)_2(OH)_6$], a mineral classified in the jarosite-alunite family and often associated with amorphous Fe/Mn phases, is another important Tl-bearing solid phase that could control the solubility of Tl in impacted areas (Xiong, 2009; Makreski et al., 2017). Although dorallcharite mineral was not identified by either XRD or SEM-EDS analyses, partial substitution of Tl in the jarosite structure is very likely considering the complete dorallcharite-jarosite solid solution and that Tl concentrates preferentially in a material of jarositic composition (Zunic et al., 1994; Aguilar-Carrillo and Herrera-García, 2018). Additionally, it has also been suggested that Tl may incorporate into the gypsum structure with Tl^+ substituting Ca^{2+} just as K^+ replaces Ca^{2+} in the $CaSO_4$ lattice due to similar charge/size ionic ratios (Lu et al., 2002; Cruz-Hernández et al., 2018). Sulfides, however, were not detected by either XRD or SEM analyses, in good agreement with the low Tl content extracted in the oxidizable fraction F4 (2.7%, Table 4, Fig. 3).

According to the elemental composition of the waste pile sample M46, Fe was the most abundant element followed by S, Zn and Mn (Table 2), as confirmed by the presence of Mn oxides (birnessite) and Zn alumino-silicate (Table 3). It is widely known that Fe/Mn oxyhydroxides, as well as Fe hydroxysulfates such as jarosite and schwertmannite, have high sorption capacities for many metals in the environment (Benjamin and Leckie, 1981; Tessier et al., 1996; Sparks, 2005; DeGraff, 2007). Recent studies carried out in areas affected by mining-metallurgical activities have demonstrated that Fe/Mn solid phases also play a pivotal role in Tl mobilization through surface complexation, oxidation, and precipitation processes, especially when poorly-crystalline phases are present (Casiot et al., 2011; Kabata-Pendias, 2011; Vanek et al., 2011; Wan et al., 2014; Li et al., 2017). As a result, Tl may be adsorbed onto the surface of these Fe/Mn poorly-crystalline minerals, or even incorporated into the structure of jarosite and birnessite (Aguilar-Carrillo and Herrera-García, 2018). For instance, Cruz-Hernández et al. (2018) found a linear correlation ($r^2 = 0.91$) between Mn and extracted Tl in this fraction in soils developed from a metallurgical site, suggesting that poorly-crystalline Mn oxides are the minerals that control the mobility of Tl due to a surface oxidation–precipitation mechanism (Peacock and Moon, 2012). Considering that the waste pile sample M46 contains an amorphous fraction of approximately 17%, along with the amounts of Fe, Mn, and S determined by XRF (Table 2), the occurrence of poorly-crystalline Fe/Mn phases such as oxyhydroxides and/or hydroxysulfates cannot be dismissed. The SEM images of the waste pile sample are displayed in Fig. 4, and mostly consist of: irregular Fe/Mn oxyhydroxides (Fig. 4,a-b), tiny Fe-rich sulfate particles forming large aggregates (Fig. 4,c-d), micron-size euhedral crystals of jarosite (Fig. 4,e-f), and layered calcium sulfate (Fig. 4,g-h), with massive quartz particles around. Therefore, results obtained here clearly support that Tl is mostly extracted in fractions F2 and F1, which target Fe/Mn poorly-crystalline oxyhydroxides and easily extractable/exchangeable Tl, respectively.

It is remarkable that the percentage of potentially mobile Tl found in the waste pile sample (M46), especially in the most labile fractions F1 and F2, corresponds to Tl concentrations well above the maximum values for non-contaminated soils established in the Mexican standard for agricultural/residential (5.2 mg kg^{-1}) and industrial areas (67 mg kg^{-1}) (SEMARNAT, 2007). However, these regulated values for Tl are extremely high in comparison to other international environmental guidelines. For instance, France and Canada's guidelines for agricultural land use are 1 mg kg^{-1} of Tl (CCME, 1999; Peter and Viraraghavan, 2005). Spain's guidelines are as low as 0.23–0.39 mg kg^{-1} for residential/agricultural areas and 2.30 mg kg^{-1} for industrial use (BOCM, 2007; BOJA, 2015). In other countries, Tl thresholds for uncontaminated areas are even smaller (Kabata-Pendias, 2011). In addition, the amount of easily exchangeable Tl (F1) from the waste pile sample M46 is extremely high (1.81 mg L^{-1}) compared to environmental standards for wastewaters (0.14 mg L^{-1}) and drinking water (0.002 mg L^{-1}) (Peter and Viraraghavan, 2005; USEPA, 2016). All these international guideline values for Tl are, at least, one order of magnitude lower in comparison to the Mexican standard (when applicable).

Regarding the streambed sediments (M47-M48), both samples showed similar Tl distribution (Table 4, Fig. 3). Thallium is mostly associated with the residual fraction (45–66%) followed by the crystalline reducible fraction (24–30%), therefore limiting its mobility and solubility. This partitioning of Tl in the streambed sediments M47-M48 is supported by the XRD analysis, showing the presence of quartz-kaolinite and jarosite as characteristic minerals in the residual and crystalline reducible fraction, respectively (Table 3). In contrast, very little amount of Tl is bound to the other fractions, with values ranging from 0.13 to 0.30 mg kg^{-1} for the exchangeable, 0.29–0.87 mg kg^{-1} for poorly-crystalline, and 0.18–0.22 mg kg^{-1} for oxidizable fraction (Table 4, Fig. 3). The lower concentration of Tl extracted from these fractions might be due to several factors. First, even though the sulfur content is above 3 wt% (Table 2), sulfides were not detected by XRD, yet sulfates such as gypsum and jarosite were (Table 3). Also, the oxidative conditions found in the experimental site may reduce the stability of sulfide mineral phases, transforming them into sulfates. Therefore, the amount of Tl that could be bound to sulfides (and other oxidizable phases like organic matter) in the sediments is negligible, as confirmed by the sequential extraction results. Second, both samples exhibited low amorphous fraction estimated by XRD (13–15 wt%), consequently diminishing the amount of poorly-crystalline Fe/Mn particles able to interact with Tl. This is especially relevant for Mn, as its concentration in the sediment samples (0.01–0.04 wt%) substantially decreased from the nearby waste pile (0.61 wt%, Table 2).

As we mentioned before, the streambed sediments are just below the Zn–Pb waste pile and receive occasional discharge streams (Fig. 2). There should be a chemical and mineralogical similarity between the sediments and the waste pile. However, according to the XRF and XRD results displayed in Tables 2 and 3, the composition of samples M46 and M47-M48 is clearly different and so is their geochemical behavior. In general, the amount of S, Mn, and Zn within the sediment samples is noticeably lower whereas there is an enrichment of Fe, As, and Pb, thus changing the mineralogy. In addition, Mn oxides are no longer detected in the sediments by means of XRD (Table 3). It is evident that one or more geochemical mechanisms are involved in the dispersion of Tl, S, Mn, and Zn from the waste pile, preventing these elements to reach the

sediments. Mechanical and chemical actions through erosion and weathering of the waste pile may release and transport high concentrations of colloid-associated metals towards nearby stream waters, promoting their dispersion from the source of contamination (Hassellov and von der Kammer, 2008). This association is very stable and effective in carrying metal(loid)s, especially considering that carriers may be composed of more than one type of mineral phases in mine-affected solid-water systems (Hamon et al., 2005; Gomez-Gonzalez et al., 2018). As a consequence, the distribution of Tl in the waste pile and sediment samples is also dissimilar (Table 4). For instance, while Tl in the waste pile is mainly extracted in the most labile exchangeable and poorly-crystalline fractions F1-F2 (152.5 mg kg^{-1}, 77%, Fig. 3), only small quantities of Tl are bound to these fractions in the sediments (0.42–1.07 mg kg^{-1}; 7–22%, Fig. 3). Prolonged leaching and washing cycles at the waste pile resulted in the solubilization and mobilization of Tl, presumably as free aqueous Tl^{+} (Yang et al., 2005), complexed as aqueous $TlSO_4^{-}$ (Xiong, 2009) and/or carried away adsorbed on colloids of Mn and Zn phases (Wong et al., 1999; Lis et al., 2003; Huangfu et al., 2017). This would explain the lower amounts of Tl, Mn, and Zn in the sediments. On the other hand, the enrichment of Fe, As, and Pb in the streambed sediments led to the formation of lead arsenate as well as jarosite compounds (Table 3), which may adsorb and incorporate Tl (Voegelin et al., 2015; Aguilar-Carrillo and Herrera-García, 2018) and could be significantly contributing to limit the solubility of Tl in the sediment-water system. Lastly, considering the average rainfall in the sampling area (304.5 mm/year), classified as a semi-arid region according to the Köppen climate classification, the weathering process is slow but steady, and significant amounts of Tl from the waste pile are still ready to be disseminated into the surrounding environment. The continuous release of these aqueous species or suspended particles to fresh-water ephemeral streams may result in mobility and transportation of Tl instead of remaining in the sediment. Therefore, more research is needed on the sorption behavior and transport of Tl associated with secondary minerals.

4. Conclusions

Mining, metallurgical and smelting activities using polymetallic sulfide-rich ore deposits containing Tl are widely located all over Mexico, in which samples from Au–Ag ores and Zn–Pb-rich deposits showed the highest amounts of Tl. Identifying the distribution of Tl in these hazardous materials is crucial to estimate its mobility and bioavailability. The results of the sequential extractions indicated significant differences in Tl contents and chemical distribution between ore concentrates, by-products, wastes, and sediments. In general, the amount of Tl in the four labile fractions –exchangeable, poorly-crystalline and crystalline reducible, and oxidizable– was very high, exceeding in all cases the maximum allowance concentration value for environmental solid samples (1 mg kg^{-1}) and showing the hazardous nature of the studied samples. The lability degree of Tl depends on both the hosting mineral and the processing method applied. Also, the variation of Tl fractionation is related to the different degree of transformation of Tl-bearing sulfides into Fe/Mn oxyhydroxides and hydroxysulfates. As a consequence, refined by-products are potentially harmful to public health and environment, so they should be frequently monitored and controlled to reduce Tl exposure.

Thallium partitioning in the waste pile is related to long-term chemical weathering and natural erosion of mineralized rocks that led to an accumulation of Tl mostly in the easily labile forms. Intermittent washing and leaching episodes promoted the release of Tl from the waste pile, likely associated with the dissemination of manganese- and zinc-rich colloidal particles with Tl attached. A side effect of Tl dissemination from the waste pile is the low concentration of Tl in the most labile fractions of the neighboring streambed sediments, in which Tl is mostly bound to the residual fraction. However, this means that significant amounts of Tl are spreading out from the waste pile and might eventually reach the municipal aquifer system. Therefore, further aqueous geochemistry is needed to track the labile Tl from the contamination source to downstream and groundwater.

It is necessary, therefore, to delve into the knowledge of the contamination source, mobilization mechanisms, dispersion pathways, and exposure to living organisms to assess the environmental impact caused by the presence of this highly-toxic element. In this regard, the role of iron and manganese secondary phases will be of significance for Tl immobilization. Lastly, this study will contribute to develop the Mexican environmental standards and guidelines for aqueous systems to include Tl as a hazardous element to be monitored, as well as to design effective remediation strategies.

Acknowledgments

This work was funded and supported by the Institute of Metallurgy (UASLP) and the Consejo Nacional de Ciencia y Tecnología (CONACyT, grant number 595019). We thank MSc. María del Carmen Ojeda and MSc. José Manuel Martínez for supplying the samples used in this study. MSc. Ainhoa Lorenzo-Merino is kindly acknowledged for her support in the preparation of the figures and providing language assistance.

Appendix A. Supplementary data

Supplementary data to this article can be found online at https://doi.org/10.1016/j.envpol.2018.10.014.

References

Ackermann, R.O., Aggarwal, S., Dixon, J.R., Fitzgerald, A.D., Hanrahan, D.C., Hughes, G.A., Kunte, A., Lovei, M., Lvovsky, K., Somani, A.H., 1999. Pollution Prevention and Abatement Handbook 1998: toward Cleaner Production. World Bank Group, Washington, D.C, 471 pp.

Aguilar-Carrillo, J., Herrera-García, L., 2018. Thallium(I) Sequestration By Fe- And Mn-Bearing Secondary Minerals: Structural Incorporation Vs Surface Sorption, Goldschmidt Abstracts.

Aguilar-Carrillo, J., Villalobos, M., Pi-Puig, T., Escobar-Quiroz, I.N., Romero, F.M., 2018. Synergistic arsenic(v) and lead(ii) retention on synthetic jarosite. I. Simultaneous structural incorporation behaviour and mechanism. Environ. Sci. Process. Impacts 20, 354–369.

Alastuey, A., Garcia-Sanchez, A., Lopez, F., Querol, X., 1999. Evolution of pyrite mud weathering and mobility of heavy metals in the Guadiamar valley after the Aznalcollar spill, south-west Spain. Sci. Total Environ. 242, 41–55.

Alvarez-Ayuso, E., Otones, V., Murciego, A., Garcia-Sanchez, A., Santa Regina, I., 2013. Zinc, cadmium and thallium distribution in soils and plants of an area impacted by sphalerite-bearing mine wastes. Geoderma 207, 25–34.

Anagboso, M.U., Turner, A., Braungardt, C., 2013. Fractionation of thallium in the Tamar estuary, south west England. J. Geochem. Explor. 125, 1–7.

Anton, M.A.L., Spears, D.A., Somoano, M.D., Tarazona, M.R.M., 2013. Thallium in coal: analysis and environmental implications. Fuel 105, 13–18.

Bacon, J.R., Davidson, C.M., 2008. Is there a future for sequential chemical extraction? Analyst 133, 25–46.

Bayliss, P., Kolitsch, U., Nickel, E.H., Pring, A., 2010. Alunite supergroup: recommended nomenclature. Mineral. Mag. 74, 919–927.

Belzile, N., Chen, Y.-W., 2017. Thallium in the environment: a critical review focused on natural waters, soils, sediments and airborne particles. Appl. Geochem. 84, 218–243.

Benjamin, M.M., Leckie, J.O., 1981. Competitive adsorption of Cd, Cu, Zn, and Pb on amorphous iron oxyhydroxide. J. Colloid Interface Sci. 83, 410–419.

Blowes, D.W., Ptacek, C.J., Jambor, J.L., Weisener, C.G., 2003. The geochemistry of acid mine drainage. In: Holland, H.D., Turekian, K.K. (Eds.), Treatise on Geochemistry. Pergamon, Oxford, pp. 149–204.

BOCM, 2007. Orden 2720/2006, 11 de agosto 2004, pp. 29–30.

BOJA, 2015. Decreto 18/2015. In: Boletín Oficial de la Junta de Andalucía, vol. 38. Junta de Andalucía, pp. 28–64.

Camizuli, E., Scheifler, R., Garnier, S., Monna, F., Losno, R., Gourault, C., Hamm, G., Lachiche, C., Delivet, G., Chateau, C., Alibert, P., 2018. Trace metals from historical mining sites and past metallurgical activity remain bioavailable to

wildlife today. Sci. Rep. 8, 3436.
Caraballo, M.A., Rotting, T.S., Nieto, J.M., Ayora, C., 2009. Sequential extraction and DXRD applicability to poorly crystalline Fe- and Al-phase characterization from an acid mine water passive remediation system. Am. Mineral. 94, 1029–1038.
Casiot, C., Egal, M., Bruneel, O., Verma, N., Parmentier, M., Elbaz-Poulichet, F., 2011. Predominance of aqueous Tl(I) species in the river system downstream from the abandoned Carnoules mine (Southern France). Environ. Sci. Technol. 45, 2056–2064.
CCME, 1999. Canadian council of ministers of the environment. In: Canadian Soil Quality Guidelines for the Protection of Environmental and Human Health: Thallium, Canadian Environmental Quality Guidelines, Winnipeg.
Clark, K.F., Fitch, D.C., 2009. Evolution of metallic deposits in time and space in Mexico. In: Clark, K.F., Salas, G.P., Cubillas Estrada, R. (Eds.), Geologia Economica de Mexico (II Edición). Asociación de Ingenieros de Minas, Metalurgistas y Geólogos de Mexico, A.C. Servicio Geológico Mexicano, pp. 62–133.
Coup, K.M., Swedlund, P.J., 2015. Demystifying the interfacial aquatic geochemistry of thallium(I): new and old data reveal just a regular cation. Chem. Geol. 398, 97–103.
Cruz-Hernández, Y., Ruiz-García, M., Villalobos, M., Romero, F.M., Meza-Figueroa, D., Garrido, F., Hernández-Alvarez, E., Pi-Puig, T., 2018. Fractionation and mobility of thallium in areas impacted by mining-metallurgical activities: identification of a water-soluble Tl(I) fraction. Environ. Pollut. 237, 154–165.
Cheam, V., 2001. Thallium contamination of water in Canada. Water Qual. Res. J. Can. 36, 851–878.
Chen, D., Wang, G., Zou, Z., Chen, Y., 2003. Lanmuchangite, a new thallium (hydrous) sulphate from Lanmuchang, Guizhou province, China. Chin. J. Geochem. 22, 185–192.
Chen, Y.H., Wang, C.L., Liu, J., Wang, J., Qi, J.Y., Wu, Y.J., 2013. Environmental exposure and flux of thallium by industrial activities utilizing thallium-bearing pyrite. Sci. China Earth Sci. 56, 1502–1509.
DeGraff, J.V., 2007. Understanding and Responding to Hazardous Substances at Mine Sites in the Western United States. Rev. Eng. Geol. XVII. Geol. Soc. Amer., Boulder, Colorado.
Dutrizac, J.E., 1997. The behavior of thallium during jarosite precipitation. Metall. Mater. Trans. B 28, 765–776.
Dutrizac, J.E., Chen, T.T., Beauchemin, S., 2005. The behaviour of thallium(III) during jarosite precipitation. Hydrometallurgy 79, 138–153.
Escarré, J., Lefèbvre, C., Raboyeau, S., Dossantos, A., Gruber, W., Cleyet Marel, J.C., Frérot, H., Noret, N., Mahieu, S., Collin, C., van Oort, F., 2011. Heavy metal concentration survey in soils and plants of the Les Malines mining district (southern France): implications for soil restoration. Water Air Soil Pollut. 216, 485–504.
Folgueras, M.B., Alonso, M., Fernandez, F.J., 2017. Coal and sewage sludge ashes as sources of rare earth elements. Fuel 192, 128–139.
Gomez-Gonzalez, M.A., Garcia-Guinea, J., Garrido, F., Townsend, P.D., Marco, J.-F., 2015a. Thallium and manganese complexes involved in the luminescence emission of potassium-bearing aluminosilicates. J. Lumin. 159, 197–206.
Gomez-Gonzalez, M.A., Garcia-Guinea, J., Laborda, F., Garrido, F., 2015b. Thallium occurrence and partitioning in soils and sediments affected by mining activities in Madrid province (Spain). Sci. Total Environ. 536, 268–278.
Gomez-Gonzalez, M.A., Villalobos, M., Marco, J.F., Garcia-Guinea, J., Bolea, E., Laborda, F., Garrido, F., 2018. Iron oxide - clay composite vectors on long-distance transport of arsenic and toxic metals in mining-affected areas. Chemosphere 197, 759–767.
Grosslova, Z., Vanek, A., Mihaljevic, M., Ettler, V., Hojdova, M., Zadorova, T., Pavlu, L., Penizek, V., Vaneckova, B., Komarek, M., Chrastny, V., Ash, C., 2015. Bioaccumulation of thallium in a neutral soil as affected by solid-phase association. J. Geochem. Explor. 159, 208–212.
Hamon, R., Batley, G.E., Casey, P., 2005. Environmental nanovectors: an emerging science area. SETAC Globe 6, 21–22.
Hassellov, M., von der Kammer, F., 2008. Iron oxides as geochemical nanovectors for metal transport in soil-river systems. Elements 4, 401–406.
Huangfu, X., Ma, C., Ma, J., He, Q., Yang, C., Jiang, J., Wang, Y., Wu, Z., 2017. Significantly improving trace thallium removal from surface waters during coagulation enhanced by nanosized manganese dioxide. Chemosphere 168, 264–271.
IPCS, 1996. International Programme on Chemical Safety, Environmental Health Criteria (EHC) 182: Thallium. World Health Organization, Geneva, Switzerland.
Jacobson, A.R., McBride, M.B., Baveye, P., Steenhuis, T.S., 2005. Environmental factors determining the trace-level sorption of silver and thallium to soils. Sci. Total Environ. 345, 191–205.
Jakubowska, M., Pasieczna, A., Zembrzuski, W., Świt, Z., Lukaszewski, Z., 2007. Thallium in fractions of soil formed on floodplain terraces. Chemosphere 66, 611–618.
Jia, Y., Xiao, T., Zhou, G., Ning, Z., 2013. Thallium at the interface of soil and green cabbage (*Brassica oleracea* L. *var. capitata* L.): soil-plant transfer and influencing factors. Sci. Total Environ. 450, 140–147.
Kabata-Pendias, A., 2011. Trace Elements in Soils and Plants. CRC Press Taylor & Francis Group, Boca Raton, FL, USA.
Karbowska, B., 2016. Presence of thallium in the environment: sources of contaminations, distribution and monitoring methods. Environ. Monit. Assess. 188.
Karbowska, B., Zembrzuski, W., Jakubowska, M., Wojtkowiak, T., Pasieczna, A., Lukaszewski, Z., 2014. Translocation and mobility of thallium from zinc–lead ores. J. Geochem. Explor. 143, 127–135.
Kazantzis, G., 2000. Thallium in the environment and health effects. Environ. Geochem. Health 22, 275–280.
Li, H., Chen, Y.H., Long, J., Li, X., Jiang, D., Zhang, P., Qi, J., Huang, X., Liu, J., Xu, R., Gong, J., 2017. Removal of thallium from aqueous solutions using Fe-Mn binary oxides. J. Hazard Mater. 338, 296–305.
Lis, J., Pasieczna, A., Karbowska, B., Zembrzuski, W., Lukaszewski, Z., 2003. Thallium in soils and stream sediments of a Zn-Pb mining and smelting area. Environ. Sci. Technol. 37, 4569–4572.
Liu, J., Wang, J., Chen, Y.H., Xie, X., Qi, J., Lippold, H., Luo, D., Wang, C., Su, L., He, L., Wu, Q., 2016. Thallium transformation and partitioning during Pb–Zn smelting and environmental implications. Environ. Pollut. 212, 77–89.
Liu, J., Luo, X.W., Wang, J., Xiao, T.F., Chen, D.Y., Sheng, G.D., Yin, M.L., Lippold, H., Wang, C.L., Chen, Y.H., 2017a. Thallium contamination in arable soils and vegetables around a steel plant A newly-found significant source of Tl pollution in South China. Environ. Pollut. 224, 445–453.
Liu, J., Wang, J., Chen, Y.H., Lippold, H., Xiao, T.F., Li, H.S., Shen, C.C., Xie, L.H., Xie, X.F., Yang, H.L., 2017b. Geochemical transfer and preliminary health risk assessment of thallium in a riverine system in the Pearl River Basin, South China. J. Geochem. Explor. 176, 64–75.
Lopez-Arce, P., Garcia-Guinea, J., Garrido, F., 2017. Chemistry and phase evolution during roasting of toxic thallium-bearing pyrite. Chemosphere 181, 447–460.
Lu, F.H., Meyers, W.J., Hanson, G.N., 2002. Trace elements and environmental significance of Messinian gypsum deposits, the Nijar Basin, southeastern Spain. Chem. Geol. 192, 149–161.
Lukaszewski, Z., Jakubowska, M., Zembrzuski, W., 2018. The mobility of thallium from bottom soil of the Silesian-Cracowian zinc-lead ore deposit region (Poland). J. Geochem. Explor. 184, 11–16.
Makreski, P., Stefov, S., Pejov, L., Jovanovski, G., 2017. Minerals from Macedonia. XXIX. Experimental and theoretical study of the vibrational spectra of extremely rare Tl-sulfate mineral from Allchar – Dorallcharite. Vib. Spectrosc. 89, 85–91.
Martín, F., García, I., Dorronsoro, C., Simón, M., Aguilar, J., Ortíz, I., Fernández, E., Fernández, J., 2004. Thallium behavior in soils polluted by pyrite tailings (Aznalcóllar, Spain). Soil Sediment Contam. 13, 25–36.
Martin, H.W., Kaplan, D.I., 1998. Temporal changes in cadmium, thallium, and vanadium mobility in soil and phytoavailability under field conditions. Water Air Soil Pollut. Pollution 101, 399–410.
Nriagu, J.O., 1998. Thallium in the Environment. Wiley, New York.
Paldyna, J., Krasnodebska-Ostrega, B., Kregielewska, K., Kowalska, J., Jedynak, L., Golimowski, J., Grobelski, T., Farbiszewska-Kiczma, J., Farbiszewska, T., 2013. The assessment of Environ. Pollut. caused by mining and metallurgy wastes from highly polluted post-industrial regions in Southern Poland. Environ. Earth Sci. 68, 439–450.
Parviainen, A., Kauppila, T., Loukola-Ruskeeniemi, K., 2012. Long-term lake sediment records and factors affecting the evolution of metal(loid) drainage from two mine sites (SW Finland). J. Geochem. Explor. 114, 46–56.
Peacock, C.L., Moon, E.M., 2012. Oxidative scavenging of thallium by birnessite: explanation for thallium enrichment and stable isotope fractionation in marine ferromanganese precipitates. Geochem. Cosmochim. Acta 84, 297–313.
Peter, A.L.J., Viraraghavan, T., 2005. Thallium: a review of public health and environmental concerns. Environ. Int. 31, 493–501.
Petersen, M.A., Libera, M.D., Jannas, R.R., Maynard, S.R., 2001. Geology of the Cerro San Pedro porphyry-related gold-silver deposit, San Luis Potosí, Mexico. In: Albinson, T., Nelson, C.E. (Eds.), New Mines and Discoveries in Mexico and Central America. Society of Economic Geologists.
Rao, C.R.M., Sahuquillo, A., Lopez Sanchez, J.F., 2008. A review of the different methods applied in environmental geochemistry for single and sequential extraction of trace elements in soils and related materials. Water Air Soil Pollut. 189, 291–333.
Rieuwerts, J.S., Mighanetara, K., Braungardt, C.B., Rollinson, G.K., Pirrie, D., Azizi, F., 2014. Geochemistry and mineralogy of arsenic in mine wastes and stream sediments in a historic metal mining area in the UK. Sci. Total Environ. 472, 226–234.
Sahuquillo, A., Rigol, A., Rauret, G., 2003. Overview of the use of leaching/extraction tests for risk assessment of trace metals in contaminated soils and sediments. Trends Anal. Chem. 22, 152–159.
Salminen, R., 2005. Geochemical Atlas of Europe. Part 1 — Background Information, Methodology and Maps. Geological Survey of Finland, Otamedia Oy.
SEMARNAT, 2007. Norma Oficial Mexicana (NOM-147-SEMARNAT/SSA1) que establece los criterios para determinar las concentraciones de remediación de suelos contaminados por arsénico, bario, berilio, cadmio, cromo hexavalente, mercurio, níquel, plata, plomo, selenio, talio y/o vanadio. Diario Oficial de la Federación, México.
Smeaton, C.M., Walshe, G.E., Fryer, B.J., Weisener, C.G., 2012. Reductive dissolution of Tl(I)-Jarosite by *Shewanella putrefaciens*: providing new insights into Tl biogeochemistry. Environ. Sci. Technol. 46, 11086–11094.
Sparks, D.L., 2005. Toxic metals in the environment: the role of surfaces. Elements 1, 193–197.
SRM, 2003. Standard Reference Material 2710 Certificate of Analysis. National Institute of Standards & Technology. https://clu-in.org/conf/tio/xrf_082808/cd/NIST-Standard-Reference-Materials/NIST_SRM_082710.pdf.
Studnicki-Gizbert, D., Schecter, D., 2010. The environmental dynamics of a colonial fuel-rush: silver mining and deforestation in new Spain, 1522 TO 1810. Environ. Hist. 15, 94–119.
Swietlik, R., Trojanowska, M., Karbowska, B., Zembrzuski, W., 2016. Speciation and mobility of volatile heavy metals (Cd, Pb, and Tl) in fly ashes. Environ. Monit. Assess. 188.

Tessier, A., Fortin, D., Belzile, N., DeVitre, R.R., Leppard, G.G., 1996. Metal sorption to diagenetic iron and manganese oxyhydroxides and associated organic matter: narrowing the gap between field and laboratory measurements. Geochem. Cosmochim. Acta 60, 387–404.

Tu, S.H., Racz, G.J., Goh, T.B., 1994. Transformations of synthetic birnessite as affected by ph and manganese concentration. Clay Clay Miner. 42, 321–330.

Ure, A.M., Quevauviller, P., Muntau, H., Griepink, B., 1993. Speciation of heavy-metals in soils and sediments - an account of the improvement and harmonization of extraction techniques undertaken under the auspices of the bcr of the commission-of-the-european-communities. Int. J. Environ. Anal. Chem. 51, 135–151.

USEPA, 2014. Priority pollutant list. United States Environmental Protection Agency. Available at. https://www.epa.gov/sites/production/files/2015-09/documents/priority-pollutant-list-epa.pdf.

USEPA, 2016. In: Drinking Water Contaminants – Standards and Regulations. United States Environmental Protection Agency. www.epa.gov/ground-water-and-drinking-water/national-primary-drinking-water-regulations#Inorganic.

Vaněk, A., Chrastný, V., Komárek, M., Penížek, V., Teper, L., Cabala, J., Drábek, O., 2013. Geochemical position of thallium in soils from a smelter-impacted area. J. Geochem. Explor. 124, 176–182.

Vaněk, A., Grösslová, Z., Mihaljevič, M., Ettler, V., Chrastný, V., Komárek, M., Tejnecký, V., Drábek, O., Penížek, V., Galušková, I., Vaněčková, B., Pavlů, L., Ash, C., 2015. Thallium contamination of soils/vegetation as affected by sphalerite weathering: a model rhizospheric experiment. J. Hazard Mater. 283, 148–156.

Vanek, A., Komarek, M., Vokurkova, P., Mihaljevic, M., Sebek, O., Panuskova, G., Chrastny, V., Drabek, O., 2011. Effect of illite and birnessite on thallium retention and bioavailability in contaminated soils. J. Hazard Mater. 191, 170–176.

Vázquez, S.E., 2012. Caracterización de un depósito no controlado de residuos mineros y evaluación de su impacto en suelo superficial: San Luis Potosí, S.L.P., México. Facultad de Ingeniería, Universidad Autónoma de San Luis Potosí, San Luis Potosí, S.L.P., México, p. 118.

Voegelin, A., Pfenninger, N., Petrikis, J., Majzlan, J., Plötze, M., Senn, A.C., Mangold, S., Steininger, R., Göttlicher, J., 2015. Thallium speciation and extractability in a thallium- and arsenic-rich soil developed from mineralized carbonate rock. Environ. Sci. Technol. 49, 5390–5398.

Wan, S., Ma, M., Lv, L., Qian, L., Xu, S., Xue, Y., Ma, Z., 2014. Selective capture of thallium(I) ion from aqueous solutions by amorphous hydrous manganese dioxide. Chem. Eng. J. 239, 200–206.

WHO/IPCS, 1996. World Health Organization/International Program on Chemical Safety). Thallium. Environmental Health Criteria, 182. World Health Organization, Geneva.

Wong, H.K.T., Gauthier, A., Nriagu, J.O., 1999. Dispersion and toxicity of metals from abandoned gold mine tailings at Goldenville, Nova Scotia, Canada. Sci. Total Environ. 228, 35–47.

Xiao, T., Guha, J., Boyle, D., Liu, C.-Q., Zheng, B., Wilson, G.C., Rouleau, A., Chen, J., 2004. Naturally occurring thallium: a hidden geoenvironmental health hazard? Environ. Int. 30, 501–507.

Xiao, T., Yang, F., Li, S., Zheng, B., Ning, Z., 2012. Thallium pollution in China: a geoenvironmental perspective. Sci. Total Environ. 421–422, 51–58.

Xiong, Y.L., 2009. The aqueous geochemistry of thallium: speciation and solubility of thallium in low temperature systems. Environ. Chem. 6, 441–451.

Yang, C.X., Chen, Y.H., Peng, P.A., Li, C., Chang, X.Y., Wu, Y.J., 2009. Trace element transformations and partitioning during the roasting of pyrite ores in the sulfuric acid industry. J. Hazard Mater. 167, 835–845.

Yang, C.X., Chen, Y.H., Peng, P.A., Li, C., Chang, X.Y., Xie, C., 2005. Distribution of natural and anthropogenic thallium in the soils in an industrial pyrite slag disposing area. Sci. Total Environ. 341, 159–172.

Zhou, J.X., Huang, Z.L., Zhou, G.F., Li, X.B., Ding, W., Bao, G.P., 2011. Trace elements and rare earth elements of sulfide minerals in the Tianqiao Pb-Zn ore deposit, Guizhou province, China. Acta Geologica Sinica-Eng. Ed. 85, 189–199.

Zunic, T.B., Moelo, Y., Loncar, Z., Micheelsen, H., 1994. Dorallcharite, Tl0.8K0.2Fe3(SO4)2(OH)6, a new member of the jarosite-alunite family. Eur. J. Mineral 6, 255–263.